

Mobility overestimation in MoS₂ transistors due to invasive voltage probes

Peng Wu^{1*}

¹Research Laboratory of Electronics, Massachusetts Institute of Technology, Cambridge, MA 02139, USA

*E-mail: pengw@mit.edu

Arising from Ng et al. *Nature Electronics* <https://doi.org/10.1038/s41928-022-00777-z> (2022)

Improving carrier mobilities of two-dimensional (2D) semiconductors is highly sought after. Recently, Ng, et al.¹ reported rippled molybdenum disulfide (MoS₂) transistors on bulged silicon nitride (SiN_x) substrates that exhibit high electron mobilities up to $\sim 900 \text{ cm}^2\text{V}^{-1}\text{s}^{-1}$. The high mobility values were attributed to the suppression of electron-phonon scattering by the lattice distortion in the rippled MoS₂ channel. While the results are compelling, this Matters Arising shows that the mobility values in ref. [1] are likely to be overestimated due to invasive voltage probes in the four-probe measurement setup, which causes a positive threshold voltage shift near the voltage probes and an artificial overestimation of apparent field-effect mobility.

Previous studies^{2,3} has shown that the gate-voltage dependent contact resistance in transition metal dichalcogenide (TMD) transistors could lead to an overestimation of mobility. In particular, ref. [3] shows that the threshold voltage V_{th} near the metal contacts shows a positive shift compared with the V_{th} in the channel region. The shift is caused by depletion of carriers near the metal contacts due to Fermi level pinning at the metal-TMD interfaces, and thus a larger gate voltage is required to populate carriers in the region (i.e., a larger V_{th}). Although a four-probe measurement setup is adopted in ref. [1] to exclude the impact of contact resistance, due to the invasiveness⁴⁻⁶ of the voltage probes (Supplementary Fig. 14a in ref. [1]), the impact of metal contacts is not completely eliminated and the regions near the voltage probes are still expected to exhibit a positive V_{th} shift (Fig. 1a).

To prove the existence of positive V_{th} shift in the MoS₂ field-effect transistor (FET), Fig. 1b shows the carrier concentrations versus gate overdrive voltage $V_G - V_{th}$ in Hall and FET measurements from Fig. 3f in ref. [1]. One can clearly see that the V_{th} from FET measurement exhibit a $\sim 25 \text{ V}$ positive shift compared with the V_{th} from Hall measurement. This is because in a two-probe FET measurement setup (or in a four-probe setup with invasive voltage probes), V_{th} is determined by

the region with the largest V_{th} , i.e., the regions near the metal contacts (or voltage probes), while in the Hall measurement, the carrier concentration is extracted from Hall resistance R_{xy} versus magnetic field B , which measures V_{th} in the channel, since the Hall voltage V_{xy} is perpendicular to the current flow and is not affected by the more resistive regions near the voltage probes (inset of Fig. 1b). Similar V_{th} discrepancies in Hall and four-probe measurements have also been observed in Supplementary Fig. 11 of ref. [7], a previous paper that also reported mobility enhancement in MoS₂ on crested SiN_x substrates.

Next, a device model that captures the V_{th} shift effect is developed. As shown in Fig. 1a, the total channel resistance is modelled as the series resistance of the two regions close to voltage probes (with a threshold voltage of V_{th1}) and the unaffected region in the channel (with a threshold voltage of V_{th2}). Since four-probe measurement is adopted, no contact resistance is considered. Therefore, the electrical conductivity of the channel σ_{ch} is given by:

$$\sigma_{ch} = [\phi\sigma_1^{-1} + (1 - \phi)\sigma_2^{-1}]^{-1} \quad (1)$$

in which ϕ is the proportion of the combined length of two regions close to voltage probes (blue regions in Fig. 1a) to the total channel length L , σ_1 and σ_2 are the conductivities of the regions close to voltage probes (blue regions in Fig. 1a) and the channel region (red region in Fig. 1a), respectively, given by⁸:

$$\sigma_i = \frac{L_i}{Wt_{body}} G_i = \frac{\mu_{model}}{t_{body}} C_{ox} \frac{nk_B T}{q} \ln \left[1 + \exp \frac{q(V_G - V_{th,i})}{nk_B T} \right], i = 1, 2 \quad (2)$$

in which $n = 1 + q^2 D_{it} / C_{ox}$ is the band movement factor, D_{it} is interface trap density. A constant mobility μ_{model} is assumed in the model. The parameters for the model are listed in Table 1.

Table 1 | Parameters for the model

$\mu_{model} = 140 \text{ cm}^2\text{V}^{-1}\text{s}^{-1}$, $C_{ox} = 22 \text{ nF/cm}^2$ (given in ref. [1]), $t_{body} = 1.4 \text{ nm}$ (bilayer MoS ₂)
$\phi = 0.1$, $V_{th1} = 1.5 \text{ V}$, $V_{th2} = -30 \text{ V}$, $D_{it} = 3.5 \times 10^{12} \text{ cm}^{-2}\text{eV}^{-1}$, $T = 300 \text{ K}$

Fig. 1c shows a comparison of modelled and experimental electrical conductivity σ_{ch} of MoS₂ versus gate voltage V_G , where the experimental data are extracted from Fig. 3b in ref. [1]. The conductivities of component segments, σ_1 and σ_2 , are also shown for comparison. One can see that

the model shows good agreement with the experimental data. The curvatures of the $\sigma_{\text{ch}} - V_G$ curve at different gate voltages are well reproduced, which proves that the model captures the essential mechanism of device operation. In addition, the $\sigma_{\text{ch}} - V_G$ curve (purple curve) exhibits a much steeper slope than the $\sigma_1 - V_G$ curve (blue curve) or the $\sigma_2 - V_G$ curve (red curve). This indicates that an overestimation of mobility is expected when extracting the apparent field-effect mobility $\mu_{\text{FE,app}}$ from the slope of the $\sigma_{\text{ch}} - V_G$ curve using:

$$\mu_{\text{FE,app}} = \frac{\partial I_D}{\partial V_G} \frac{1}{V_{\text{DS}}} \frac{1}{C_{\text{ox}}} \frac{L}{W} = \frac{\partial \sigma_{\text{ch}}}{\partial V_G} \frac{1}{V_{\text{DS}}} \frac{1}{C_{\text{ox}}} t_{\text{body}} \quad (3)$$

Fig. 1d shows a comparison of modelled and experimental $\mu_{\text{FE,app}}$ of MoS₂ versus V_G , where the experimental data are extracted from Fig. 3b in ref. [1] and the modelling results are calculated using eq. (3). The modelled $\mu_{\text{FE,app}}$ shows good agreement with experimental data across different V_G ranges, with the only exception of from 20 V to 30 V. Note that $\mu_{\text{FE,app}}$ exceeds the actual mobility used in the model, $\mu_{\text{model}} = 140 \text{ cm}^2\text{V}^{-1}\text{s}^{-1}$, which highlights the mobility overestimation in the measurement. Moreover, even with a constant μ_{model} , the interplay of σ_1 and σ_2 at different V_G in the model can readily explain the change of $\mu_{\text{FE,app}}$ over a broad range of V_G (except for from 20 V to 30 V), without involving a complicated transitioning between different dominant scattering mechanisms at different V_G range that is proposed in ref. [1], thus providing a simpler and more natural explanation⁹ to experimental observations. Note that similar trends of $\mu_{\text{FE,app}}$ change with V_G were also observed in ref. [7], which also indicates a possible mobility overestimation.

Finally, to provide readers a guidance on mobility measurement using four-probe measurement, different configurations of four-probe measurement are compared in Fig. 2. Previous discussion in this study mainly focuses on the first configuration with invasive voltage probes, in which the voltage probes extend over the entire channel width direction and cause the largest disturbance to the current flow and voltage distribution in the channel. Therefore, the first configuration is not recommended for four-probe measurement, although it can be used in transfer length method¹⁰ (TLM) to more reliably exclude the impact of metal contacts.

The second configuration with partially invasive voltage probes is adopted in part of the results in ref. [1] (Fig 3a and Supplementary Fig. 21 in ref. [1]). However, the voltage probes still disturb the current flow and voltage distribution in the channel, and the measured longitudinal voltage V_{xx}

may pick up signals from the voltage drop in the more resistive depletion regions near the voltage probes, and thus the measurement is still prone to mobility overestimation as discussed before. That being said, this configuration may still be adopted if one tries to minimize the overlap between the voltage probes and the channel^{3,11} and reduce the disturbance from the voltage probes as much as possible.

The third configuration with non-invasive voltage probes is most recommended for four-probe measurement. In this configuration, the impact of voltage probes to the current flow and voltage distribution in the channel is minimized, although the device fabrication is more complicated as it involves etching the channel into a Hall bar geometry¹².

In conclusion, the mobility values reported in ref. [1] (and in a previous paper⁷) are likely to be overestimated due to the impact of invasive voltage probes in the four-probe measurement. A device model that captures the impact of the metal contacts is developed, which achieves good agreement with the experimental data while providing a simple and convincing explanation for the apparent field-effect mobility ($\mu_{FE,app}$) change with gate voltage.

References:

1. Ng, H. K. *et al.* Improving carrier mobility in two-dimensional semiconductors with rippled materials. *Nat. Electron.* (2022). doi:10.1038/s41928-022-00777-z
2. Nasr, J. R., Schulman, D. S., Sebastian, A., Horn, M. W. & Das, S. Mobility Deception in Nanoscale Transistors: An Untold Contact Story. *Adv. Mater.* **31**, 1806020 (2019).
3. Pang, C. *et al.* Mobility Extraction in 2D Transition Metal Dichalcogenide Devices—Avoiding Contact Resistance Implicated Overestimation. *Small* **17**, 2100940 (2021).
4. Huard, B., Stander, N., Sulpizio, J. A. & Goldhaber-Gordon, D. Evidence of the role of contacts on the observed electron-hole asymmetry in graphene. *Phys. Rev. B* **78**, 121402 (2008).
5. Blake, P. *et al.* Influence of metal contacts and charge inhomogeneity on transport properties of graphene near the neutrality point. *Solid State Commun.* **149**, 1068–1071 (2009).
6. Karnatak, P. *et al.* Current crowding mediated large contact noise in graphene field-effect transistors. *Nat. Commun.* **7**, 13703 (2016).
7. Liu, T. *et al.* Crested two-dimensional transistors. *Nat. Nanotechnol.* **14**, 223–226 (2019).
8. Khakifirooz, A., Nayfeh, O. M. & Antoniadis, D. A Simple Semiempirical Short-Channel MOSFET Current–Voltage Model Continuous Across All Regions of Operation and Employing Only Physical Parameters. *IEEE Trans. Electron Devices* **56**, 1674–1680 (2009).
9. Mazin, I. Inverse Occam’s razor. *Nat. Phys.* **18**, 367–368 (2022).
10. Cheng, Z. *et al.* How to Report and Benchmark Emerging Field-Effect Transistors. *arXiv:2203.16759*, 1–25 (2022).
11. Ber, E., Grady, R. W., Pop, E. & Yalon, E. Pinpointing the Dominant Component of Contact Resistance to Atomically Thin Semiconductors. *arXiv:2110.02563*, 1–22 (2021).
12. Cui, X. *et al.* Multi-terminal transport measurements of MoS₂ using a van der Waals heterostructure device platform. *Nat. Nanotechnol.* **10**, 534–540 (2015).

Competing interests:

The authors declare no competing interests.

Additional information:

Correspondence and requests for materials should be addressed to P.W.

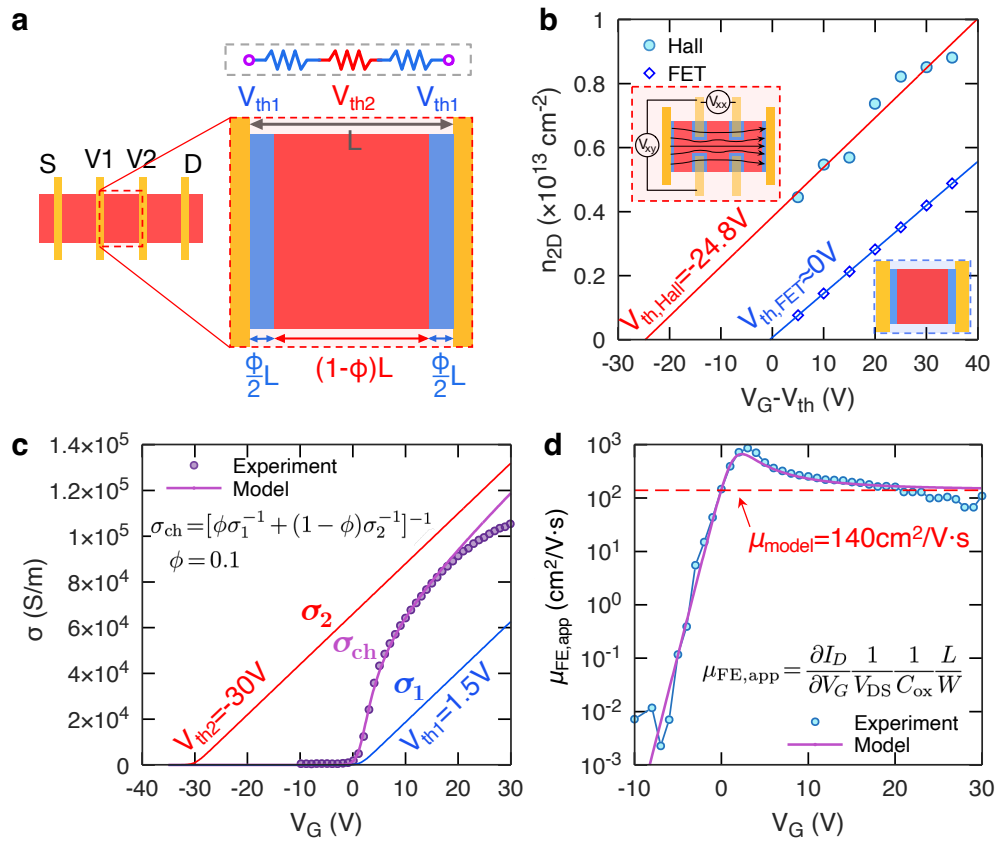


Fig. 1 | Mobility overestimation due to invasive voltage probes and threshold voltage shift. **a**, Schematic of four-probe measurement setup and illustration of threshold voltage shift caused by the invasive voltage probes. **b**, Carrier concentrations versus gate overdrive voltage in Hall and FET measurements. Experimental data are extracted from Fig. 3f in ref. [1]. **c**, Modelled and experimental electrical conductivity of MoS₂. Inset shows the threshold voltage distribution in the channel used in the model. Experimental data are extracted from Fig. 3b in ref. [1]. **d**, Modelled and experimental apparent mobility of MoS₂. Experimental data are extracted from Fig. 3b in ref. [1].

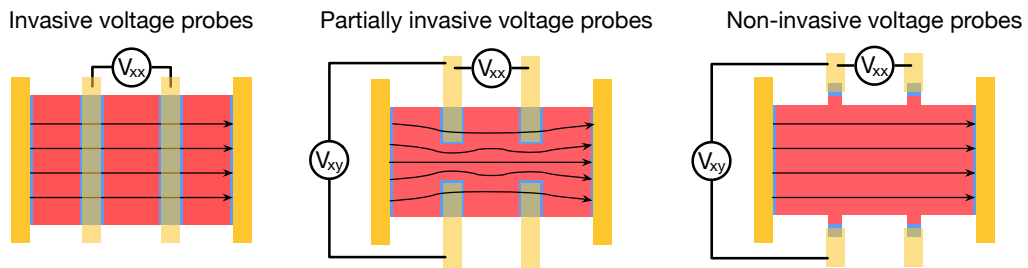


Fig. 2 | Comparison of different configurations of four-probe measurement.